Extending a Hodgkin-Huxley Model for Larval Drosophila Muscle Excitability via Particle Swarm Fitting

Extending a Hodgkin-Huxley model for larval *Drosophila* muscle excitability via particle swarm fitting

Paul Piho[1], Filip Margetiny[2], Ezio Bartocci[4], Richard R Ribchester[2,3], Jane Hillston[1]

[1] School of Informatics, University of Edinburgh, UK
[2] Centre for Discovery Brain Sciences, University of Edinburgh, UK
[3] Euan MacDonald Centre for Motor Neurone Disease Research, University of Edinburgh, UK
[4] Faculty of Informatics, TU Wien, Vienna, Austria

Abstract. We present a model of excitability in larval *Drosophila* muscles. Our model was initially based on modified Hodgkin-Huxley equations, adapted to represent variable, regenerative depolarisations (action potentials) we have occasionally observed in intracellular recordings and that can be triggered by excitatory junction potentials at neuromuscular synapses. We modified several kinetic equations describing voltage sensitive Ca^{2+} and K^{+} ionic currents, previously used to predict excitability in muscle cells of the mammalian cardiac atrioventricular node. The resulting nonlinear differential equations had multiple unknown parameters. Thus, to fit the model to experimental observations of variable excitability, we developed a new implementation of particle swarm optimisation. This GPU-based implementation allows us to adopt an ensemble model approach in which each experimental observation is used to find a plausible parameterisation, resulting in a set of models accounting for cell-to-cell variability of muscle excitability in *Drosophila* larvae, and with potential applications to population-based modeling of other excitable cell types.

1 Introduction

The control of muscle contraction is fundamental to behaviour. In mammals and other vertebrates, muscle contraction is the end result of a signalling cascade that begins with excitation of motor neurones in the brain stem or spinal cord, triggering waves of regenerative depolarization and repolarization (action potentials) that are propagated by saltatory conduction along each myelinated nerve axon. Activation of muscle fibres takes place at neuromuscular junctions (NMJs). When a muscle action potential is propagated along the muscle surface membrane it leads to conformational change in muscle proteins, enabling contraction.

In this paper we investigated the mechanisms of muscle excitability in the abdominal muscles of larval fruit flies (*Drosophila melanogaster*). These invertebrate muscles do not express the voltage-sensitive sodium channels that are

essential for generation of action potentials in vertebrate muscle fibres. Larval muscles do, however, contain voltage-sensitive calcium (Ca^{2+}) and potassium (K^+) channels: a similar situation to some non-skeletal muscle fibres in vertebrates, for example in the atrioventricular (AV) node of the mammalian heart [8, 3, 12]. However, unlike mammalian cardiac AV node cells, the functional significance of voltage-sensitive Ca^{2+} and K^+ channels in larval *Drosophila* muscle fibres is unclear, since activation of these channels is not necessary for muscle contraction and the summative effects of a short burst of excitatory NMJ potentials (EJPs) is sufficient for evoking contractile responses [22, 14]. Nevertheless, larval *Drosophila* muscle fibres are capable of regenerative, Ca^{2+}-dependent depolarization and we seek to establish the physiological role of these phenomena. As part of that ongoing investigation, we have developed a computational model of excitability at larval *Drosophila* NMJs. Our approach was initially based on a modified Hodgkin-Huxley model of the firing properties of muscle cells in the mammalian cardiac AV node, which also depends mainly on a combination of interacting voltage-sensitive Ca^{2+} currents and K^+ currents [8]. In addition, in order to parameterise the model we have applied a new GPU-based implementation of the particle swarm optimisation method, following a similar procedure to others [15]. Initial investigations of this model suggest that the quantitative characteristics of the regenerative responses that have been observed experimentally can be accounted for by a computational model of this type.

The rest of the paper is structured as follows. In Section 2 we present an overview of the relevant biological background and a brief summary of Hodgkin-Huxley models of action potentials. In Section 3 we introduce the computational model of excitability at larval *Drosophila* neuromuscular junctions. In Section 4 we set up the parameter study for the presented model in the context of particle swarm optimisation and describe the preprocessing steps taken for isolating individual examples of actions potentials from the experimental data. In Section 5 we discuss the results of the parameter fitting for the considered model and finally, in Section 6 we give conclusions and some further research directions.

2 Background

2.1 Action potentials

Action potentials are primary mechanisms of cell-to-cell communication in nervous and neuromuscular systems and they occur when transmembrane voltage undergoes rapid depolarisation then repolarisation. In neurones, this is often referred to as spiking or firing. The changes in membrane potential are caused by the flow of charged ions along their extracellular-intracellullar concentration gradients through voltage-gated ion channels in the cell membrane, proteins that typically incorporate selectivity filters for Na^+, Ca^{2+} or K^+ ions. In the resting state, the inside voltage is often more negative than $-70mV$ with respect to the outside, due to the open states of voltage-insensitive channels. The opening of voltage-sensitive channels becomes regenerative when membrane potential is depolarised beyond critical threshold values that are unique for each type of

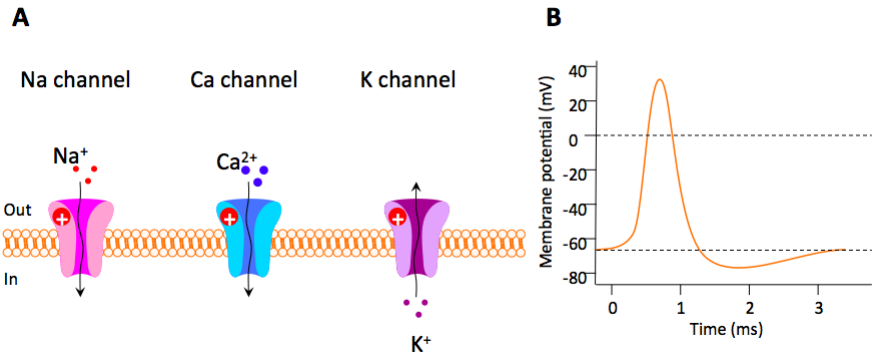

Fig. 1: A. Voltage sensitive ion channels in excitable cell membranes with the normal direction of ionic flux when open indicated. Several subtypes of Na, Ca and K channels are expressed in different cell types and species, differing in protein structure and activation/inactivation kinetics. B. Schematic illustration of regenerative depolarization (action potential) and recovery of the transmembrane resting potential following activation of ion channels like those shown in A. The magnitude and time course of these phenomena vary between cell types, depending on the number, density and types of voltage-sensitive ion channels.

channel protein. Opening of Na^+ or Ca^{2+} channels admits positively charged ions into the cell, further depolarising the membrane and causing more channels to open. This positive feedback is frequently sufficient to bring about a rapid reversal in the membrane potential (inside becoming positive, rather than negative). The polarity of the membrane is then restored by a combination of delayed voltage-dependent inactivation and delayed activation of other channels, typically K^+-channels, that enable flux of positive ions along concentration gradients from inside to out. This interplay between ion channels of different types is the basis of the depolarization/repolarization that is used to propagate signals along axons and between cells (Figure 1).

In vertebrate skeletal muscle, action potentials are trigged by axonal contacts at neuromuscular junctions (NMJs). Each presynaptic motor nerve terminal contains neurotransmitter molecules (acetylcholine) packaged into 30 nm spheres (synaptic vesicles), some of which are tethered to the intracellular surface nerve membrane at "active zones". An incoming nerve action potential triggers fusion of about 50 vesicles with the nerve terminal membrane, releasing their contents into the synaptic cleft. This process of exocytosis is executed following influx of Ca^{2+} ions through Ca^{2+}-selective, voltage sensitive ion channels in the nerve terminal membrane. These ions then bind to signaling proteins integrated into the active zone molecular complex [23, 24]. Molecules of neurotransmitter released by exocytosis diffuse rapidly across the narrow (50 nm) synaptic cleft between motor nerve terminal and muscle fibre, where they bind to specific protein receptors located in high density ($> 10^5$ μm^{-2}) at the crests of mem-

brane folds of the motor endplate, the muscle surface opposed to the sites of presynaptic neurotransmitter release. Activation of these receptors generates an inward postsynaptic ionic current, which depolarizes the motor endplate membrane. When the membrane potential at the motor endplate reaches around $-65\ mV$, voltage-sensitive Na-channels (NaV channels) located in the crypts of the junctional folds are activated, leading to a regenerative depolarization that is similar in character to the neuronal action potential [30, 29, 11]. The muscle action potential is propagated along the muscle surface membrane and into a network of invaginations known as t-tubules. Here, proteins are coupled to those controlling the release of Ca^{2+} from the sarcoplasmic reticulum, an intracellular membrane-bound storage depot [4]. Binding of released Ca^{2+} brings about an energy-dependent conformational change in other muscle proteins, enabling force generation or muscle shortening via recycling of molecular cross-bridges between an orderly array of cytoskeletal filaments comprising the protein molecules actin and myosin [26]. Neuromuscular function is similarly initiated and executed in invertebrate muscles, including those of *Drosophila* larvae. The most distinctive chemical and structural differences are that larval NMJs utilise glutamate as a neurotransmitter and the postsynaptic membrane folds, rich in glutamate receptors, are more extensive than in vertebrates and is normally referred to as the sub-synaptic reticulum.

Action potentials in vertebrate muscle fibres are obligatory for excitation-contraction coupling: if NaV channels in muscle are selectively blocked pharmacologically, then synaptically-evoked endplate potentials (EPPs) at neuromuscular junctions, though tens of millivolts in amplitude, fail to trigger muscle contraction [29, 17]. By contrast, muscle fibres in the abdominal muscles of larval *Drosophila*, do not express NaV channels. Instead, they contain voltage-sensitive Ca^{2+} and K^+ channels. But as noted above, the functional significance of voltage-sensitive Ca^{2+} and K^+ channels in larval *Drosophila* muscle fibres is unclear. It is generally regarded that they are of little physiological significance since they are only reliably observed in recordings from muscles in which extracellular Ca^{2+} concentration is increased beyond normal physiological maxima, or when membrane K^+ permeability is reduced by adding selective channel blocking drugs [22, 10, 21, 6].

However, action potentials are also occasionally observed in larval muscle fibres under more normal physiological recording conditions [25, 31]. Figure 2(A) shows an intracellular microelectrode recording obtained from a filleted preparation of a 3rd instar larval *Drosophila*, which clearly shows a train of spikes: regenerative depolarising action potentials. Larval fillet preparations and intracellular recordings were made using standard techniques [27]. The preparation was bathed in a normal HL3.1 physiological saline (containing $1.5\ mM\ Ca^{2+}; 4\ mM\ Mg^{2+}$) without any ion channel blockers. The muscles were impaled with glass microelectrodes, resistance $10 - 40 M\Omega$. Segmental nerves were aspirated into a fire-polished $10\mu m$ diameter suction pipette/electrode and stimulated with 0.2ms pulses 1-10V in amplitude. Trigger and current pulses were delivered and recordings were captured via a Digidata 1550B interface using pClamp-10 software

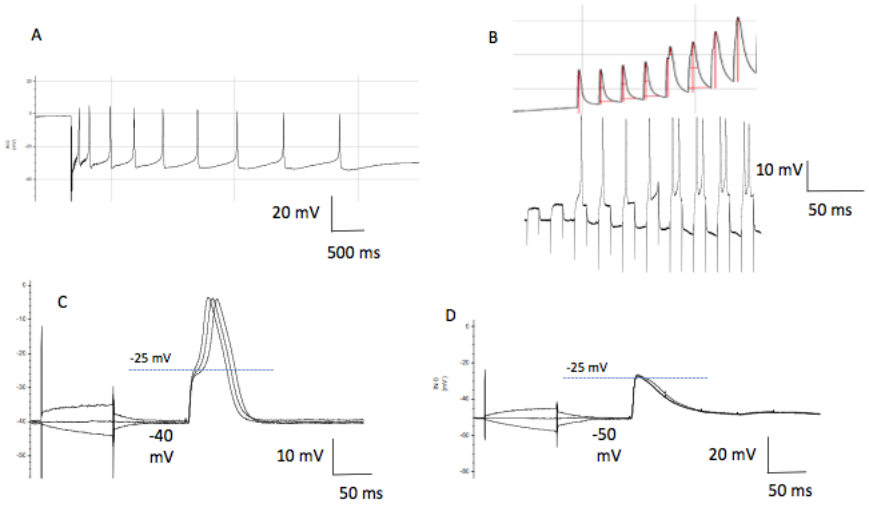

Fig. 2: Trace obtained during impalement of Muscle 4, in normal HL3.1 bathing medium and in the absence of any ion channel blockers. B. Combined optical recording of twitch contractions (arbitrary units) of Muscle 12 in a 3rd instar larval fillet preparation (upper trace) and simultaneous intracellular recording of membrane potential in response to progressive 2nA increments in the strength of current pulses injected through the recording microelectrode (lower trace) in normal HL3.1 medium. Baseline drift was due to slight movement of the preparation during recording. C: Intracellular recording of a nerve-evoked excitatory synaptic (junctional) potential (EJP) in Muscle 6, sufficient to activate a regenerative action potential (three successive sweeps at 2s intervals). D: Spontaneous hyperpolarisation of the resting potential by about 10 mV, in the same muscle fibre as C, abolished the regenerative depolarisation, leaving only a large EJP in response to nerve stimulation. The prepulses in C,D are responses to ± 1 nA rectangular pulses injected through the recording microelectrode, used to check membrane integrity (resistance and capacitance).

(Molecular Devices, San Jose, USA). Images were captured using a QImaging Optimos camera (Teledyne Photometrics, Tucson, USA) driven by public domain Micromanager software (micro-manager.org). Images were postprocessed and muscle contractions recording in FiJi (imagej.net/Fiji) using the Muscle Motion plugin (github.com/l-sala/MUSCLEMOTION).

A brief discharge of action potentials diminished in frequency as the resting membrane potential spontaneously hyperpolarised. The identified muscle in this case was Muscle 4 but we have observed similar phenomena in intracellular recordings from muscles 5, 6, 7, 12, and 13. Figure 2(B) shows combined optical recording of twitch contractions of Muscle 12 in 3rd instar larval fillet

preparation (upper trace) and simultaneous intracellular recording of membrane potential in response to progressive $2nA$ increments in the strength of current pulses injected through the glass recording microelectrode (lower trace), in normal HL3.1 medium. Contractile responses were only elicited when membrane depolarisation exceeded the firing threshold for regenerative responses. Summative contractile responses were evoked when membrane depolarisation was sufficient to evoke action potential doublets.

The experience from the Ribchester Lab is that about 10% of freshly-dissected larval preparations bathed in normal (or even reduced) Ca^{2+} containing media show action potentials and these are associated with brisk muscle contractions (c.f. Figure 2(B)). The mechanism of these regenerative responses, which activate at a much higher threshold than vertebrate muscle action potentials, is wholly consistent with published data on the voltage-dependence of Ca^{2+} channels and K^{+}-channels expressed in larval muscle: specifically, a form of L-type Ca^{2+} channel with an activation threshold of about $-25mV$, as well as several types of K^{+}-channels [21, 6]. Sixteen of these recordings were from muscle fibres that showed sufficient membrane integrity and stability to warrant further analysis and simulation.

2.2 Hodgkin-Huxley type models

In 1952 Hodgkin and Huxley proposed and tested a model to account for the propagation of action potentials in the squid giant axon, the most favourable preparation at that time for comparing empirical data with computational analysis [7]. The Hodgkin-Huxley formulation was based on the notion that membrane ionic permeability is voltage- and time-dependent and that permeabilities to ions, specifically Na^{+} and K^{+}, are associated with distinct activation and inactivation kinetics. In their model, the cell membrane is represented as a dielectric separating conducting ionic media, thus conferring transmembrane capacitance, in parallel with batteries representing transmembrane voltages. Selective ionic permeabilities were represented by separate variable conductances. Based on this abstraction they applied and numerically solved a set of nonlinear ordinary differential equations (ODEs) to describe the flow of membrane current and to predict the change in transmembrane voltage during the action potential [7].

The voltage-sensitive ionic permeabilities envisaged by Hodgkin and Huxley were subsequently shown to be mediated by protein molecules embedded in membranes and that functioned as ion channels in their open state [18]. Subsequently such models were adapted to other excitable cell types, including cardiac and skeletal muscle, and are now widely used in membrane biophysics due to their computational efficiency and relative mathematical simplicity.

2.3 Particle swarm optimisation

PSO is a stochastic optimisation technique for continuous non-linear functions introduced by Eberhart and Kennedy in [5] and is inspired by social behaviour of

bird flocking or fish schooling. The algorithm initialises and maintains a swarm of particles where each particles represents a random solution with a velocity in the search space. Each particle moves through the search space based on its own the best solution, and the best global solution, obtained thus far. It was demonstrated in [32] that a GPU based implementation can result in performance improvements for large swarm sizes and many dimensional problems.

3 Model

The structure of the model presented here is based on a Hodgkin-Huxley type model [7] of myocyte action potentials in the AV node of the mammalian heart published by Inada *et al.* [9]. We based the model on nodal cells of myocardium, as we hypothesised the same ionic properties (Ca^{2+} : K^+ gating) underlie the generation of action potentials in larval *Drosophila* muscle. Our model assumed one cellular compartment (inside-outside) and was modified to accommodate different kinetics appropriate to the larval muscle fibres. Functional homologues for channels known to occur in *Drosophila* muscle but which are absent from the cardiac muscle were added.

The model represents the change in voltage across the cell membrane based on the temperature, membrane capacitance and atmospheric pressure (all treated as constants and specified in Appendix A) and a sum of ionic currents flowing through open ion channels. The total voltage change was determined as a function of ionic current based on the following equation

$$\frac{d}{dt}V = \frac{-I_{total}}{C_m} + \frac{d}{dt}V_{init}, \qquad I_{total} = I_{Cv} + I_{Kv1} + I_{Kv2} + I_{Kv3} + I_b + I_f$$

giving the change in membrane voltage as a function of time and ionic currents in *Drosophila* muscle cells. V_{init} is a function representing the magnitude and time course of initial depolarisation that results from activation of ligand-gated glutamate channels by neurotransmitter at the NMJs and which then triggers activation of the voltage-gated currents. This function aims to account for the dataset consisting of evoked responses as the synaptic signal which it represents is not integral to action potential occurrence but is present in our dataset.

Ion channels in the model are characterised using sets of ODEs, which are used to determine the expected proportion of channels which are in open (conducting) state, as opposed to closed (non-conducting) states. The proportion of channels in the open state is dependent on their activation and inactivation rates as a function of membrane voltage, values of which are dependent on a set of equations expressing sensitivity of the channel to voltage and time.

The total current passing through the ion channels is dependent on the conductance of ion channels which represents the population of channels present on the cell surface. In this paper, we explore different parametrisations of the conductance values to identify the channels which contribute the most to the characteristics of the *Drosophila* muscle action potential.

The model under consideration consists of 6 ion channels and the initialisation current – one channel (Cv2) modelling the inward currents, three (Kv1, Kv2, Kv3) modelling the outward current and finally two pacemaking currents (I_b, HCN) modelling channels which conduct inwards at highly negative membrane voltages and outwards in more positive voltages. The ODE formulations of the channels, along with their empirically found parametrisations of the activation and inactivation rates, are from papers [9] and [1]. In the following we give a brief description of the channels and their functions in the model. The ODE formulations of the channels are given in Appendix A.

Cv2 current The channel gives the inward Ca^{2+} current underlying muscle activation in *Drosophila* embryos. The formulation of Cv2 model was taken from the model of rabbit atrioventricular cell by Inada *et al.* [9], due to their functional resemblance to mammalian L-type channels.

Kv1 current (Shaw) Kv1 channel in *Drosophila* larvae conducts a transient outward potassium current. It is a voltage dependent, fast inactivating potassium channel, which controls (and prevents) repetitive firing of the cell by prolonging and enhancing hyperpolarisation of the cell in response to depolarisation. The formulation for Kv1 current used in this paper taken from its mammalian homologue in rat Purkinje cell neurons[1].

Kv2 current (Shab) Kv2 carries a delayed-rectifier potassium current. The channel slowly opens and closes in response to depolarising voltage. The delayed activation kinetics are important to control the duration of action potential in 3rd instar *Drosophila* and mammalian neurons. The formulation of Kv2 current considered here was taken from [9] formulation for IKr.

Kv3 current (Shaker) Kv3 channels are low conductance ion channels activated at depolarised voltages which generate atypical, delayed voltage-dependent slowly activating and non-inactivating currents. These contribute to maintaining of the resting membrane potential but have little effect on action potential parameters. In traditional Hodgkin-Huxley type models these channels could be considered K^+ leak channels. As for Kv1 current the formulation for Kv3 is modelled after its mammalian homologue Kv3.3 from rat Purkinje cells [1].

Background current I_b As there is only one type of functional voltage-gated excitatory ion channel, with relatively high activating threshold (around $-25mV$), in order to observe spontaneous action potentials a depolarising driving force (pacemaker current) is necessary. The formulation for fast pacemaking background current was taken from rabbit heart background pacemaker as in [9].

HCN current I_f In previous versions (Margetiny, unpublished), the fits of the model to experimental data were seen to improve when an HCN channel (or channel with HCN-like kinetics) was added. However, whether or not such a channel occurs in *Drosophila* muscle tissue is unknown. We consider the original model from rabbit cardiomyocyte [9] in the context of regenerative responses in *Drosophila* muscles. Similarly to background current, HCN is hypothesised to be a multiple-ion permeable channel, albeit with much slower kinetics.

Initialisation current The initialisation current is modelled through its time-dependent effect on the voltage by

$$V_i(t) = \beta_i \left(\frac{t}{\alpha_i}\right) \exp\left(1 - \frac{t}{\alpha_i}\right)$$

4 Parameter estimation problem

The general parameter estimation problem we are aiming to solve is the following: what are the parameters $\boldsymbol{\theta}$ such that the deterministic model $f(t, \boldsymbol{\theta})$ serves as a good predictor to the voltage response during an action potential as observed in the experimental time-series data. In the following we describe the available experimental data as well as the preprocessing steps.

4.1 Data preprocessing

The available data is in the form of time series measurements of voltage response to stimulus provided by current injections. Figures 3a and 3b give two examples of available time series. Figure 3a shows the voltage response to a single induced synaptic stimulus triggering an action potential while Figure 3b shows five consecutive stimuli. Note that in this case only one of the current injections has triggered the action potential behaviour.

The measurements from the experiments started with a depolarising current intended to test the membrane resistance and is not relevant to the fitting of the model (c.f. Figure 2(C)). The timings for testing the membrane resistance are consistent throughout the dataset and thus we have simply dropped measurements before 0.2 seconds. For hence forward we are considering the time series with the prepulse removed.

From there, we need to identify the parts of the time series corresponding to the action potential behaviour. The method for identifying parts of the time series is done in the following way. For each time series

- we identify the indices $\{i_1, \cdots, i_n\}$ corresponding to peaks in the time series using standard implementations of peak finding algorithms.
- we identify the indices $\{j_1, \cdots, j_n\}$ corresponding to where the peaks start. For that we first use Savgol-Goyal high pass filter [19] to smooth the time series resulting in a series for which we can numerically calculate derivatives. Working backwards from a peak we find where the derivatives change sign.
- we split the time series into n parts corresponding to single instances of action potentials in the following way. The k-th series corresponds to the values of the original time series between the indices j_k and j_{k+1}. We normalise the time by taking the initial time to be 0.0. For each point between j_k and j_{k+1} we consider the time passed since the measurement at index j_k. Secondly, we normalise voltages by considering the voltage differences between the base of the peak at index j_k each point in the new time series.

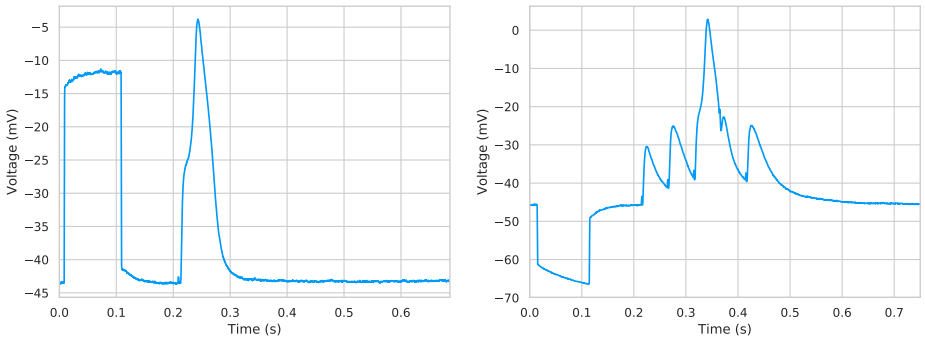

(a) Response to a single synaptic (NMJ) stimulus, triggering a regenerative response (same recording as Figure 2C). Prepulse is a membrane resistance test pulse.

(b) Five consecutive synaptic stimuli, only the third of which triggered as regenerative response

Fig. 3: Time series data for voltage response during action potential.

- Note that not all such generated time series correspond to action potentials. We pick a threshold voltage of $-10mV$ for the peaks that are likely to correspond to the action potential phenomenon.
- In order to reduce the computational load we are going to consider a subsample of the generated time-series.

Figure 4 gives examples of the results of the process. In particular, the dots represent an 18 point sub-sample of the experimental time series showing the action potential. The number of sampling points is an arbitrary choice and can be easily changed as long as the sub-sample sufficiently captures the shape characteristics of the traces. The resulting dataset from the available recordings consists of 16 instances of action potentials.

4.2 PSO fitting

For this preliminary study of fitting the Hodgkin-Huxley type action potential model we used a standard particle swarm optimisation (PSO) algorithm over a given search space. The fitness calculations are given by the following. Given a single action potential time series consisting of points $(t_0, V_0), \cdots, (t_m, V_m)$ and a model $f(t, \boldsymbol{\theta})$ parametrised by $\boldsymbol{\theta}$ we consider the simple distance measure

$$K(\boldsymbol{\theta}) = \sum_{i=0}^{m} \left(f(t_i, \boldsymbol{\theta}) - f(0, \boldsymbol{\theta}) - V_i\right)^2$$

where $f(t_i, \boldsymbol{\theta}) - f(0, \boldsymbol{\theta})$ gives the difference of the voltages predicted by the model at time 0 and t_i and V_i gives the same quantity for the experimental time

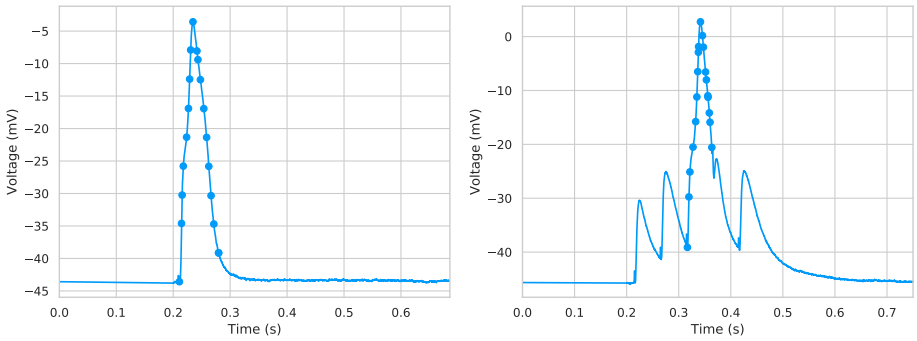

(a) Single synaptic response same as Fig. 3a)

(b) Consecutive synaptic responses (same recording as Fig. 3b)

Fig. 4: Generated time-series sub-sampled at 18 points.

series. Similarly to the multi-swarm method presented in [15] we perform the optimisation algorithm for multiple initialisations of the swarm. In our case the initialisations are provided by the distinct time-series of action potentials.

4.3 Implementation

The standard PSO algorithm adapted for the described problems proceeds through the following steps:

1. Particles are initialised with uniformly sampled values from the search space and velocities. An alternative initialisation of particles through Latin hypercube sampling, as done in [20] can be considered in further work.
2. For each particle the set of ODEs giving the corresponding system dynamics is solved.
3. Based on the ODE solutions each particle gets a reward value.
4. Global maximum reward is found.
5. The location of a particle, $\boldsymbol{\theta}$, in the search space is updated based on the global maximum $\boldsymbol{\theta}_{\text{gbest}}$ and individual best previous location of the particle $\boldsymbol{\theta}_{\text{ibest}}$. In particular, the update between the i-th and $(i+1)$-th iteration for an individual particle takes the following form

$$\boldsymbol{\theta}_{i+1} = \boldsymbol{\theta}_i + w\boldsymbol{v}_i + c_1 r_{i_1}(\boldsymbol{\theta}_{\text{ibest}_i} - \boldsymbol{\theta}_i) + c_2 r_{i_2}(\boldsymbol{\theta}_{\text{gbest}_i} - \boldsymbol{\theta}_i)$$

   where r_{i_1}, r_{i_2} are random numbers in the interval $[0, 1]$ and w (weight given to previous velocities), c_1 (called cognitive weight) and c_2 (called social weight) are parameters of the optimisation algorithm.
6. Go back to Step 2.

In the implementation we made use of the fact that PSO is easily parallelisable on graphics processing units (GPUs) [32, 15] so that each particle is assigned a single GPU thread. In particular, for the standard PSO given above all steps other than Step 2 are easily parallelisable. Reward evaluations are slightly more complex consisting of two steps: the integration step for solving the system of ODEs and the actual reward calculation. However, storing the trajectories resulting from numerical integration in memory would severely limit the scalability of the algorithm to large numbers of particles. Instead, we can update the value of the reward function on the fly after each step of the numerical integration. This way only the point necessary for the next iteration of numerical integration is stored in memory. The integration for reward calculations in this paper was performed by the simple Euler forward method. For the model presented in this paper this was found to be sufficient but other fixed time-step methods, like Runge-Kutta fourth-order method, can be easily considered. Finally, the boundary conditions are enforce in the following way: if the particle is about to violate the boundary for a given parameter its position in the component of this parameter is set to the boundary value while reversing the relevant component of its velocity.

5 Results

The parameters under investigation are the conductance values for each of the channels ($g_{Cv}, g_{Kv1}, g_{Kv2}, g_{Kv3}, g_{I_b}, g_f$), the reversal potential E_b for the background pacemaker current and the shape parameters α_i, β_i for the voltage change due to the initial current injection. The bounds for each of the parameter values are set to encompass a range of physiologically plausible values. For conductances this was the interval between $0.0\mu S$ and $0.016\mu S$. The viable shape parameters for the initialisation current were set so that the induced voltage would reach its peak between values 10 mV and 25 mV before $0.5ms$ in order to feasibly set up the action potential. We conducted two sets of experiments: a) parameter g_f was held at 0.0 ,disabling the channel in the model and b) the HCN channel corresponding to g_f conductance values was enabled. For both sets of experiments we ran the PSO on the action potential traces 6 times – each with different random seeding and a varying weight parameter w from $\{0.7, 0.72, 0.74, 0.76, 0.78, 0.80\}$ to further perturb the behaviour of the particle swarms between different experiments in order to find as many different optima as possible. We set the values $c_1 = c_2 = 2.0$ as in [5]. The effect of varying the social and cognitive weights for this problem was not explored and is left for further work. We ran a fixed number (2000) of iterations. Little can be said about the convergence properties of the PSO for the given fitness function, but in experiments we saw that 2000 iterations generally allowed the swarms to settle to some local optimal values.

In the multi-swarm implementation we associated each instance of observed action potential with its own fitness function. Not averaging over the collected AP samples and running the PSO algorithm on each sample multiple times allows us to effectively find a set of plausible parametrisations of the proposed model. This gives an alternative way to generate a population of models aiming to take

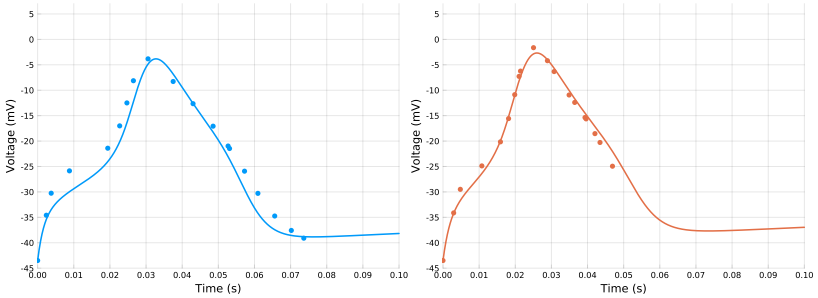

Fig. 5: Blue and red trajectories correspond to best model fittings for the time-series presented in Figure 4. a) and b) respectively.

Table 1: Mean and standard deviation of fitted conductance values for the model with the HCN channel disabled.

	mean	std.		mean	std.
g_{Cv2}	0.0106	0.0031	g_{Kv3}	0.0083	0.0053
g_{Kv1}	0.0093	0.0043	g_b	0.0102	0.0038
g_{Kv2}	0.0091	0.0041	E_b	2.8	23.4

into account the cell-to-cell variability similarly to [2] [13]. Figure 5 shows the model fitted to sub-samples of the time series shown in Figure 4. The results of the fitting are summarised by combined box and violin plots in Figures 6 and 7, describing the shape of the distributions of found parameter values. Table 1 gives mean and standard deviation summary statistics for the model fitting with the HCN channel disabled. We have discarded parameters which give rise to voltage responses that do not recover to the interval $-50mV$ to $-30mV$ after the occurrence of an action potential or result in overly low fitness values.

From the results of parameter fitting with HCN channel disabled we first note that the summary plots indicate that conductance values of g_{Cv2} and g_b close to 0 are unlikely to fit the experimental traces well. This seems to confirm the necessity for involvement of both Cv2 channels and a pacemaker current I_b to facilitate action potentials in *Drosophila*. In addition, slightly tighter interquartile range for the Kv2 channel conductance compared to the other two K^+ channels (Kv1, Kv3) points towards its more significant effect in shaping of the action potentials while Kv1 and Kv3 are permitted to vary more. This is consistent with previously understood physiology of *Drosophila* muscle ionic activity as Kv1 and Kv3 are expected to be important in regulation of repeated firing and unlikely to influence the parameters of a single action potential. Surprisingly, the modelling experiments might indicate a higher reversal potential for I_b than originally expected (median $-1.5\ mV$ with mean $2.8\ mV$ and standard deviation 23.4, as opposed to $-22\ mV$). A higher reversal potential for I_b may suggest a more complex current consisting of several ion channel conductances, or a single channel which is more biased towards inward current than previously estimated. This inspires further modelling and experimental enquiry

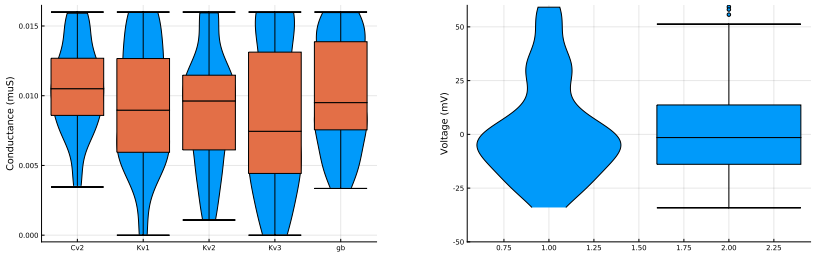

(a) Conductances (b) Background current reversal potential.

Fig. 6: Violin and box plots of fitted parameter values for the model the HCN channel disabled.

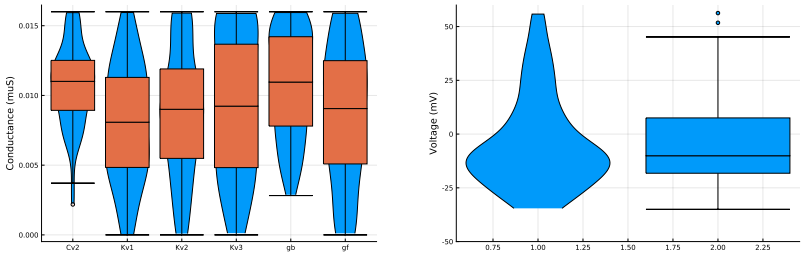

(a) Conductances (b) Background current reversal potential.

Fig. 7: Violin and box plots of fitted parameter values for the model including the HCN channel.

into the nature of channel or channels responsible for the generation of background pacemaking current. Further, we experimented with addition of HCN channels. The resulting dispersion of fitted conductance values g_f is similar to Kv1 and Kv3 indicating that the presence of the HCN channel in the model is of little importance for fitting *Drosophila* action potentials. Moreover the fitness calculations do not show quantitatively better fits being achieved with the addition of the HCN channel.

All optimisation runs were conducted with 2000 iterations where a swarm of 64 particles was assigned to each of the 16 trajectories, thus simulating 1024 particles in parallel. Each run took approximately 4 minutes to complete on a machine equipped with Nvidia Titan X GPU with the equivalent single-threaded execution on a laptop CPU taking around 19 minutes. Additionally, the GPU implementation provided better scalability for the same optimisation problem, with the total of 2048 and 4096 particles taking 7 and 12 min in the case of the GPU implementation and 38 and 78 min in the case of the CPU implementations.

6 Conclusion

We have presented a new model of excitability of the abdominal muscles of larval *Drosophila*, observed experimentally following excitatory depolarisation at

a minority of NMJs, and used this model to explore techniques for modulation of its parameters via a novel GPU-based implementation of the particle swarm optimisation method. This approach was computationally very efficient and supported an ensemble model view, allowing each action potential recording to be used to obtain a plausible set of parameters that might be used, for example, to account for cell-to-cell variability in the incidence, magnitude and time course of regenerative action potentials in larval muscle recordings.

From a functional standpoint, our unpublished preliminary data suggest that when freely moving larvae undergo rapid peristaltic locomotion, for example to escape a potential predator there is insufficient time for more than one brisk and powerful twitch contraction per abdominal segment. Combined measurements of synaptic potentials and muscle shortening indicate that single EJPs are not sufficient to account for this escape behaviour (M.Fjeldstad and R.R.Ribchester, *unpublished*). Thus, we hypothesise that rapid contractile responses of larval muscle fibres are enabled by an endogenous mechanism that modulates the muscle fibre resting membrane potential and this permits synaptic depolarization to trigger a regenerative response (Figure 2 (C,D)). This results, as in vertebrate muscle, in brisk muscle contraction (Figure 2 (B)). This hypothesis implies that further analysis of the characteristics and mechanism of regenerative membrane depolarization in larval *Drosophila* muscle will yield deeper insight into their function. Computational modelling of these events and exploring the scope and causes of their variability from moment to moment will facilitate the analysis.

Due to the nature of the model, distinct channels expressed in the model are capable of compensating for each other resulting in widely dispersed viable parameter values. Thus analysis of correlations between the parameter values as well as refinements and alterations of the model would be of interest for further work. In many such scenarios the small size of the currently available dataset would be a limiting factor. On a practical level, dynamic modelling (including parameter fitting) in real time would be a valuable tool that could complement experimental approaches, such as the dynamic clamp technique: an experimental procedure that enables electrophysiologists to explore the consequences and potential functional significance of varying the specificity and kinetics of different ionic currents and determining their transitory effects on membrane potential [28, 16]. Computational speed is an essential consideration for real time feedback between dynamic modelling and dynamic clamp to be feasible and practical.

Acknowledgements

We thank Mr Keiran Brown for assistance with intracellular recordings and Professor Mark Boyett, Manchester University, for sharing source code for action potential modelling in myocytes of the rabbit AV node. FM is supported by an MRC PhD Studentship in the University of Edinburgh Doctoral Training Programme in Precision Medicine. PP is supported by EPSRC grant EP/L01503X/1 (CDT in Pervasive Parallelism) and STSM Grant from COST Action IC1406 High-Performance Modelling and Simulation for Big Data Applications.

References

1. Akemann, W., Knöpfel, T.: Interaction of Kv3 potassium channels and resurgent sodium current influences the rate of spontaneous firing of Purkinje neurons. Journal of Neuroscience **26**(17), 4602–4612 (2006). https://doi.org/10.1523/JNEUROSCI.5204-05.2006
2. Britton, O.J., Bueno-Orovio, A., Van Ammel, K., Lu, H.R., Towart, R., Gallacher, D.J., Rodriguez, B.: Experimentally calibrated population of models predicts and explains intersubject variability in cardiac cellular electrophysiology. Proceedings of the National Academy of Sciences **110**(23), 2098 –2015 (2013). https://doi.org/10.1073/pnas.1304382110
3. Choisy, S., Cheng, H., Orchard, C., James, A., Hancox, J.: Electrophysiological properties of myocytes isolated from the mouse antrioventricular node: L-type ICA, IKr, If, and Na-Ca exchange. Physiol Rep **3**, e12633 (2015)
4. Dulhunty, A.: Excitation-contraction coupling from the 1950s to the new millenium. Clin. Exp. Pharmacol. Physiol. **33**, 763–772 (2006)
5. Eberhart, R., Kennedy, J.: A new optimizer using particle swarm theory. In: MHS'95. Proceedings of the Sixth International Symposium on Micro Machine and Human Science. pp. 39–43 (Oct 1995). https://doi.org/10.1109/MHS.1995.494215
6. Gielow, M., Gu, G., Singh, S.: Resolution and pharmacological analysis of the voltage-dependent clacium channels of *Drosophila* larval muscles. J. Neurosci. **15**, 6085–6093 (1995)
7. Hodgkin, A., Huxley, A.: A quantitative description of membrane current and its application to conductance and excitation in nerve. J. Physiology **11**(4), 500–544 (1952)
8. Inada, S., Hancox, J., Zhang, H., Boyett, M.: One-dimensional mathematical model of the atrioventricalur node including atrio-nodal, nodal and nodal-His cells. Biophys. J. **97**, 2117–2127 (2009)
9. Inada, S., Hancox, J., Zhang, H., Boyett, M.: One-dimensional mathematical model of the atrioventricular node including atrio-nodal, nodal, and nodal-His cells. Biophysical Journal **97**(8), 2117–2127 (Oct 2009). https://doi.org/10.1016/j.bpj.2009.06.056
10. Lee, J., Ueda, A., Wu, C.: Distinct roles of *Drosophila* cacophany and Dmca1D Ca(2+) channels in synaptic homeostasis: genetic interactions with slowpoke Ca(2+)-activated BK channels in presynaptic excitability and postsynaptic response. Dev. Neurobiol. **74**, 1–15 (2014)
11. Martin, A.: Amplification of neurotransmission by postjunctional folds. Proc. Biol. Sci. **258**, 321–326 (1994)
12. Munk, A., Adjemian, R., Zhao, J., Ogbabhebriel, A., Shrier, A.: Electrophysiological prperties of morphologically distinct cells isolated from the rabbit atrioventricular node. J. Physiol. (Lond.) **493**(Pt 3), 801–818 (1996)
13. Muszkiewicz, A., Britton, O.J., Gemmell, P., Passini, E., Sánchez, C., Zhou, X., Carusi, A., Quinn, T.A., Burrage, K., Bueno-Orovio, A., Rodriguez, B.: Variability in cardiac electrophysiology: Using experimentally-calibrated populations of models to move beyond the single virtual physiological human paradigm. Progress in biophysics and molecular biology **120**(1-3), 115—127 (January 2016). https://doi.org/10.1016/j.pbiomolbio.2015.12.002
14. Newman, Z., *et al.*: Input-specific plasticity and homeostasis at the *Drosophila* larval neuromuscular junction. Neuron **93**, 1388–1404 (2017)

15. Nobile, M.S., Besozzi, D., Cazzaniga, P., Mauri, G., Pescini, D.: A GPU-based multi-swarm PSO method for parameter estimation in stochastic biological systems exploiting discrete-time target series. In: EvoBIO 2012, Málaga, Spain, April 11-13, 2012. Proceedings. pp. 74–85 (2012). https://doi.org/10.1007/978-3-642-29066-4_7
16. Ortega, F., Butera, R., Christini, D., White, J., Dorval, A.: Dynamic clamp in cardiac and neuronal systems using RTXI. Methods Mol. Biol. **1183**, 327–354 (2014)
17. Ribchester, R., *et al.*: Progressive abnormalities in skeletal muscle and neuromuscular junctions of trangenic mice expressing the Huntingdon's disease mutation. The European Journal of Neuroscience **20**, 3092–3114 (2004)
18. Sakmann, B., Neher, E.: Patch clamp techniques for studying ionic channels in excitable membranes. Annu. Rev. Physiol. **46**, 455–472 (1984)
19. Savitzky, A., Golay, M.J.E.: Smoothing and differentiation of data by simplified least squares procedures. Analytical Chemistry **36**, 1627–1639 (1964)
20. Schutte, J.F., Reinbolt, J.A., Fregly, B.J., Haftka, R.T., George, A.D.: Parallel global optimization with the particle swarm algorithm. International Journal for Numerical Methods in Engineering **61**(13), 2296–2315 (2004). https://doi.org/10.1002/nme.1149
21. Singh, S., Wu, C.: Properties of potassium currents and their role in membrane excitability in *Drosophila* larval muscle fibers. J. Exp. Biol. **152**, 59–76 (1990)
22. Singh, S., Wu, C.: Ionic currents in larval muscles of *Drosophila*. Int. Rev. Neurobiol. **43**, 191–220 (1999)
23. Slater, C.: The functional organization of motor nerve terminals. Prog. Neurobiol. **134**, 55–103 (2015)
24. Südof, T.: Neurotransmitter release: the last millisecond in the life of a synaptic vesicle. Neuron **80**, 675–690 (2013)
25. Suzuki, N., Kano, M.: Development of action potential in larval muscle fibers in *Drosophila melanogaster*. J. Cell. Physiol. **93**, 383–388 (1977)
26. Sweeney, H., Hammers, D.: Muscle contraction. Cold Spring Harbour Perspect. Biol. **10**, a023200 (2018)
27. West, R.J.H., Briggs, L., Perona Fjeldstad, M., Ribchester, R.R., Sweeney, S.T.: Sphingolipids regulate neuromuscular synapse structure and function in drosophila. Journal of Comparative Neurology **526**(13), 1995–2009 (2018). https://doi.org/10.1002/cne.24466
28. Wilders, R.: Dynamic clamp: a powerful tool in cardiac electrophysiology. J. Physiol. (Lond) **576**, 349–359 (2006)
29. Wood, S., Slater, C.: The contribution of postsynaptic folds to the safety factor for neurotrnsmission in rat fast- and slow-twitch muscles. J. Physiol. (Lond) **500 (Part 1)**, 165–176 (1997)
30. Wood, S., Slater, C.: Safety factor at the neuromuscular junction. Prog. Neurobiol. **64**, 393–429 (2001)
31. Yamaoka, K., Ikeda, K.: Electrogenic responses elicited by transmembrane depolarizing current in aerated body wall muscles of *Drosophila melanogaster* larvae. J. Comp. Physiol. **163**, 705–714 (1988)
32. Zhou, Y., Tan, Y.: Gpu-based parallel particle swarm optimization. In: Proceedings of the IEEE Congress on Evolutionary Computation, CEC 2009, Trondheim, Norway. pp. 1493–1500 (2009). https://doi.org/10.1109/CEC.2009.4983119

Appendix A Model

The following appendix gives the ODE formulations of the channels considered in this paper. The ODEs are characterised by general Hodgkin-Huxley scheme, with a transitions between channels in open and shut states modelled as a first order chemical reaction

$$\text{open} \underset{\beta}{\overset{\alpha}{\rightleftarrows}} \text{shut}$$

Transition rate expressions α and β provided for the channels in this model correspond to number of openings or closures of channel per second.

The functions for d_{L_∞}, m_∞, n_∞, y_∞ determine the proportion of channels in a particular (generally open) state under equilibrium conditions. This value changes as a function of the membrane voltage via a change in voltage dependent rates α and β. While change in equilibrium proportion happens instantly, change in real proportion of channels in open state does not: the rate at which the proportion of d_L, m, n, d, y changes towards its equilibrium value is given by a differential equation. The time constant τ is an expression of how fast this equilibrium is achieved and is dependent on the innate properties of channel and its sensitivity to voltage. Channels Cv1 and Kv2 have more than one inactivation mode – one happening at a slower time-scale than the other. These are denoted $f_{L,fast}$, $f_{L,slow}$ for the Cv1 channel and $p_{a,fast}$ and $p_{a,slow}$ for the Kv2 channel.

Reversal potential E_K for potassium and calcium calcium channels at temperature $294.15K$ (laboratory conditions) were calculated using the Nernst equation based on expected intracellular and extracellular concentrations of potassium and calcium

$$E = \frac{RT}{zF} \ln \frac{[\text{ion concentration ouside}]}{[\text{ion concentration inside}]}$$

where R is the universal gas constant, T the temperature in Kelvins, F the Faraday constant and z valency of the ion. For *Drosophila* the intracellular concentrations are estimated to be 0.05 $mmol$ and 140 $mmol$ for calcium and potassium respectively. Extracellular solution for the experiments used 5.0 $mmol$ potassium and 1.5 $mmol$ calcium concentration. Finally, Q_{10} is experimentally [1] determined time change constant for the Kv1 potassium channel.

Background current I_b

$$I_b(V) = g_b(V - E_b)$$

HCN current I_f

$$y_\infty(V) = \frac{1.0}{1.0 + \exp(\frac{V+83.19}{13.56})} \qquad \frac{d}{dt}y = \frac{y_\infty - y}{\tau_y}$$

$$\tau_y(V) = 0.250 + 2.0\exp(-\frac{(V+70.0)^2}{500.0}) \qquad I_f(V) = g_f y(V - E_f)$$

Cv1 current

$$d_{L\infty}(V) = \frac{1}{1 + \exp\left(\frac{V+18.2}{-5}\right)} \qquad \frac{d}{dt}d_L = \frac{d_{L\infty} - d_L}{\tau_{d_L}}$$

$$\alpha_{d_L}(V) = \frac{-26.12(V+35.0)}{\exp\left(\frac{V+35.0}{-2.5}\right) - 1} \qquad \frac{d}{dt}f_{L,fast} = \frac{f_{L,fast\infty} - f_{L,fast}}{\tau_{L,fast}}$$

$$+\frac{-78.11V}{\exp(-0.208V) - 1} \qquad \frac{d}{dt}f_{L,slow} = \frac{f_{L,slow\infty} - f_{L,fast}}{\tau_{L,slow}}$$

$$\beta_{d_L}(V) = \frac{10.52(V-5.0)}{\exp(0.4 \times (V-5.0)) - 1.0} \qquad \tau_{d_L} = \frac{1}{\alpha_{d_L} + \beta_{d_L}}$$

$$I_{Cv2}(V) = g_{Cv} d_L (0.675 f_{L,fast} + 0.325 f_{L,slow})(V - E_{CaL})$$

Kv2 current

$$p_{a,fast\infty}(V) = \qquad p_{i\infty}(V) = \frac{1}{1 + \exp\left(\frac{V+4.9}{15.14}\right)} \times$$

$$p_{a,slow\infty}(V) = \frac{1}{1 + \exp\left(\frac{V+10.22}{-8.5}\right)} \qquad \left(1 - 0.3\exp\left(\frac{-V^2}{500}\right)\right)$$

$$\tau_{p_{a,fast}(V)} = \frac{1}{\begin{array}{r}17\exp(0.0398V) + \\ 0.221\exp(-0.051V)\end{array}} \qquad \alpha_{p_i}(V) = 92.01\exp(-0.0183V)$$

$$\beta_{p_i}(V) = 603.6\exp(0.00942)$$

$$\tau_{p_{a,slow}(V)} = 0.33581$$

$$+0.90673\exp\left(\frac{-(V+10.0)^2}{988.05}\right) \qquad \tau_{p_i} = \frac{1}{\alpha_{p_i} + \beta_{p_i}}$$

$$\frac{d}{dt}p_{a,fast} = \frac{p_{a,fast\infty} - p_{a,fast}}{\tau_{p_{a,fast}}} \qquad \frac{d}{dt}p_i = \frac{p_{i\infty} - p_i}{\tau_{p_i}}$$

$$I_{Kv2}(V) = g_{Kv2}\left(0.9p_{a,fast} + 0.1p_{a,slow}\right)p_i(V - E_K)$$

Kv1 current

$$\alpha_n(V) = 0.12889 \exp\left(\frac{-V + 45.0}{-33.90877}\right)$$

$$\beta_n(V) = 0.12889 \exp\left(\frac{-V + 45.0}{12.42101}\right)$$

$$n_\infty(V) = \frac{\alpha_n(V)}{\alpha_n(V) + \beta_n(V)}$$

$$\tau_n = Q_{10} \frac{1}{\alpha_n + \beta_n}$$

$$\frac{d}{dt} n = \frac{n_\infty - n}{\tau_n}$$

$$I_{Kv1} = g_{Kv1} n^4 (V - E_K)$$

Kv3 current

$$\alpha_{mShaw}(V) = 0.22 \exp\left(\frac{V + 16}{26.5}\right)$$

$$\beta_{mShaw}(V) = 0.22 \exp\left(\frac{-V + 16}{26.5}\right)$$

$$m_\infty(V) = \frac{\alpha_n}{\alpha_n + \beta_n}$$

$$\tau_{mShaw} = \frac{1}{\alpha_{mShaw} + \beta_{mShaw}}$$

$$\frac{d}{dt} m = \frac{m_\infty - m}{\tau_{mShaw}}$$

$$I_{Kv3} = g_{Kv3} m^4 (V - E_K)$$